ROYAL SOCIETY
OF CHEMISTRY

PAPER

Check for updates

Glyme-based liquid–solid electrolytes for lithium metal batteries†

M. Nojabaee, [ID] J. Popovic [ID] * and J. Maier

The development of stable electrolytes for lithium metal batteries is urgently required. In this work, nanoporous alumina/lithium salt-containing glyme liquid–solid composite electrolytes are proposed. The beneficial interfacial effect and transport properties such as ionic conductivity and lithium transference number can be tuned by variation of the cell temperature and electrolyte salt concentration. In symmetrical lithium/electrolyte/lithium cells, glyme-based liquid–solid electrolytes show superior performance compared to their liquid counterparts. However, even in the high lithium transference number cases, unfavorable mossy lithium deposits can be observed.

1. Introduction

Ever since the discovery of the lithium ion batteries, lithium metal has been envisaged as an optimal anode due to the highest theoretical capacity (3860 mA h g^{-1}) and the lowest electrochemical potential (−3.04 V *vs.* hydrogen electrode).[1–5] On the other hand, lithium metal is particularly interesting for the development of the so-called next generation Li–S and Li–O$_2$ battery technologies.[6,7] Key challenges in lithium metal batteries are poor safety and cycleability, a consequence of the instable solid electrolyte interphase (SEI) forming between the typical electrolytes and the lithium anode, as well as deposition of lithium in mossy or dendritic form.[8,9] Recently, a number of solutions have been proposed, including chemical or physical pre-treatment of the lithium metal to form an artificial SEI,[10–14] homogenization of the Li-ion flux,[15–17] tuning of the shear modulus of the electrolyte and application of external pressure,[18–22] as well as electrolyte composition adaptation.[23–27]

An interesting class of materials, suggested to be useful in lithium metal batteries, are liquid/solid (hybrid) electrolytes, created by infiltration of salt-in-solvent electrolytes into nanoporous solid matrix.[28–31] Appropriate liquid/solid electrolytes offer high ionic conductivities accompanied with good adhesion properties, and high shear modulus. Solids which offer beneficial surface adsorption properties are able to immobilize the anions on the surface, locally enhance the Li$^+$ conductivity and boost the lithium transference number without compromising overall conductivity.[32–34] Such liquid/solid electrolytes have the potential to enable dendrite-free lithium metal batteries at lower currents.[35,36]

Max Planck Institute for Solid State Research, Stuttgart, Germany. E-mail: popovic@fkf.mpg.de

In this work, we report on anodic aluminium oxide (AAO) membranes infiltrated with glyme-based lithium electrolytes as potential candidates for lithium metal batteries. AAO membranes are chosen as they offer well-defined porosities with small enough pore size, while glyme-based electrolytes already showed good stability *vs.* lithium electrode.[34,37] We investigate systematically how the changes in temperature and salt concentration influence interfacial effects and transport properties such as ionic conductivity and lithium transference number. Finally, we investigate the failure mechanism of the Li|liquid/solid electrolyte|Li cells as well as the structure of the lithium deposits formed during lithium/stripping plating experiments.

2. Experimental

Characterization of the anodic aluminum oxide (AAO)

The morphology of the AAO monoliths (diameter, d = 13 mm, thickness t = 60 μm, Whatman Anodisc® purchased from Sigma-Aldrich) was observed using scanning electron microscopy (SEM, Zeiss Merlin device operating at 5 kV). The samples were coated with a conducting carbon layer prior to the SEM measurement. The X-ray diffraction pattern was obtained in ambient environment using a Philips device with Cu Kα 1 (λ = 0.154 nm) radiation. Magic angle spinning (MAS) NMR measurements were performed on a Bruker Avance III 400 MHz instrument in a magnetic field of 9.4 T, with a Larmor frequency of 400.1 Hz for ^{1}H at room temperature and a spinning speed of 12 500 Hz. A N$_2$ adsorption–desorption apparatus (BELSORP-mini II, Bel Japan Inc.) was employed to characterize the porosity of the AAO membranes. Prior to the measurement, samples were degassed overnight at 120 °C under vacuum. Brunauer–Emmet–Teller method was used to calculate the surface area from the N$_2$ desorption curve. The ion exchange capacity (IEC) of the –OH groups in AAO was

This journal is © The Royal Society of Chemistry 2019

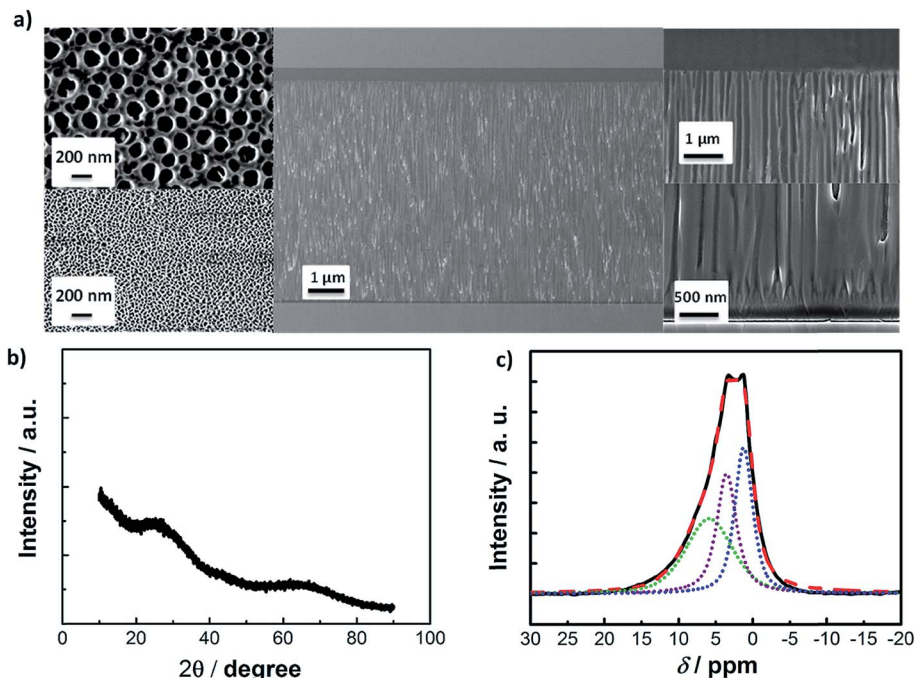*J. Mater. Chem. A*, 2019, 7, 13331–13338 | 13331

Fig. 1 Characterization of the AAO membranes: (a) scanning electron micrographs of lower and upper part of the membrane are shown on the far left. The cross-section of the pores can be seen in the center and on the right side, (b) X-ray diffraction pattern of one membrane revealing the amorphous structure of the material, (c) ^{1}H MAS-NMR spectra of a crushed membrane (black line) was fitted (dotted lines) to estimate the total number of available surface −OH groups.
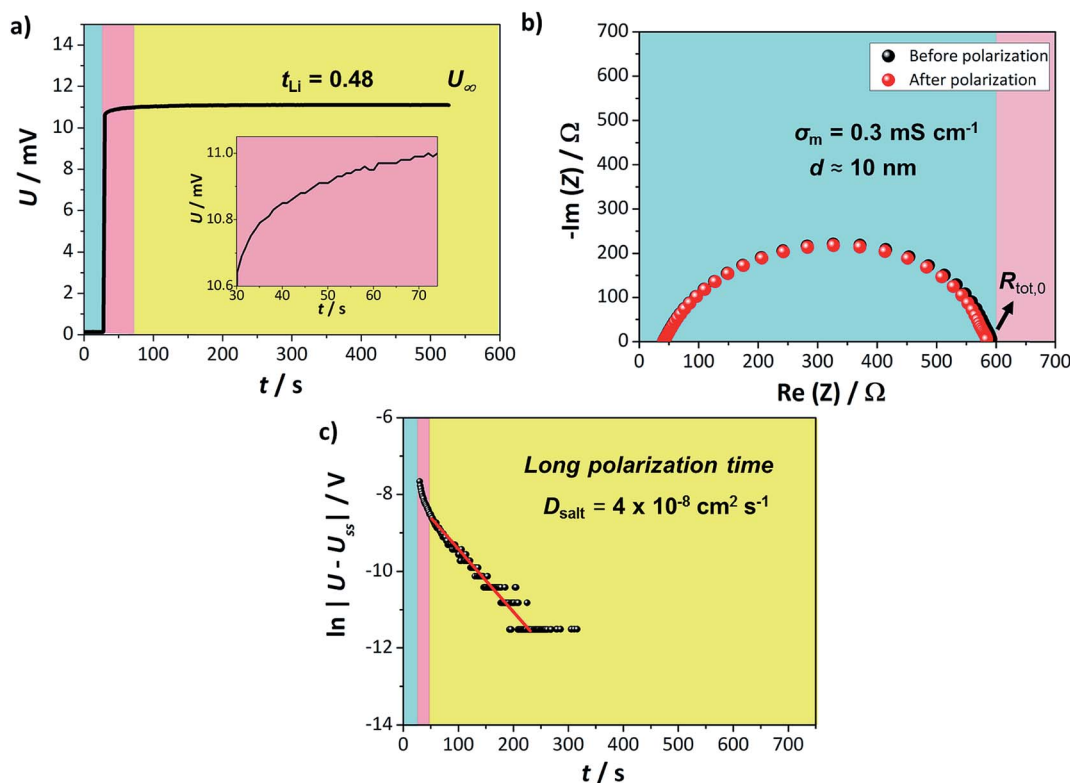

Fig. 2 Lithium transference number determination for AAO: (1 M LiTf/triglyme) in an anion blocking Li|electrolyte|Li cell. The colors (green, pink, yellow) represent different time regimes. (a) Time dependent galvanostatic polarization curve. The steady state is reached already after *ca.* 200 s. The inset shows voltage evolution for short polarization times, (b) impedance spectra recorded before (black) and after (red) the galvanostatic polarization. Observed semicircle corresponds to the unchanged solid electrolyte interphase (SEI) resistance, (c) extraction of the salt diffusion coefficient from the long polarization times.

13332 | *J. Mater. Chem. A*, 2019, **7**, 13331–13338

This journal is © The Royal Society of Chemistry 2019

calculated from the potentiometric titrations. For that purpose, a defined amount of crushed AAO particles was dispersed in a 0.1 M NaCl aqueous solution, stirred continuously for 1 h, and subsequently titrated by a 0.01 M NaOH solution, followed by back-titration with a 0.01 HCl solution up to the neutral pH values.

Electrolyte preparation

The composite electrolytes were prepared by infiltration of dry nanoporous AAO with a solution of 0.02–1 M lithium tri-fluoromethanesulfonate ($LiCF_3SO_3$, Sigma-Aldrich, 99.995%, LiTf) in tri(ethylene glycol)dimethyl ether ($M_w = 178.2$ g mol^{-1}, Sigma-Aldrich, triglyme) overnight. Triglyme solvent was distilled prior to use, and the water content of the final electrolyte thus kept below 150 ppm.

Electrolyte characterization

For the electrochemical measurements, the electrolytes were sandwiched between two symmetric lithium electrodes in a self-designed copper-plated polytetrafluorethylen (PTFE) cell. Impedance spectroscopy was applied before and after galvanostatic polarization in the frequency range from 10^{-1} to 10^7 Hz (0.1 V amplitude) using a Solartron 1260 frequency analyzer. When needed, the temperature was externally controlled by a RC6CP Lauda thermostat. The ionic conductivities were calculated from the cell geometry and the obtained resistances. The lithium plating/stripping experiments and the galvanostatic polarization measurements were performed with a Keithley 2604B source-meter instrument. Thermal properties of the electrolytes were determined using a differential scanning calorimeter (DSC 214, Polyma, Netzsch) in the temperature range from -100 °C to 80 °C at a heating rate of 10 °C min^{-1} under continuous nitrogen purging rate of 60 mL min^{-1}. Zeta potential was measured at room temperature in a closed vessel, by measuring the magnitude and phase of the Colloid Vibration Current (CVI) at 3 MHz, using an electroacoustic spectrometer (DT-1200, Dispersion Technology, Inc., Quantachrome). Electrolyte preparation and the electrochemical measurements (excluding the temperature dependent measurements and zeta potential measurements) were performed in a glovebox (<0.1 ppm H_2O, ≤0.1 ppm O_2) under Ar atmosphere.

Lithium dendrite characterization

Upon disassembling the cell in the Ar-filled glovebox, visible brown discolorations (dendrites) inside and on the top of AAO were collected and either deposited on scanning electron microscopy (SEM) sample holders or crushed, dispersed in ethanol and subsequently deposited on carbon grids for transmission electron microscopy (TEM) measurements. TEM measurements were performed using a Philips, CM200 instrument at low energies.
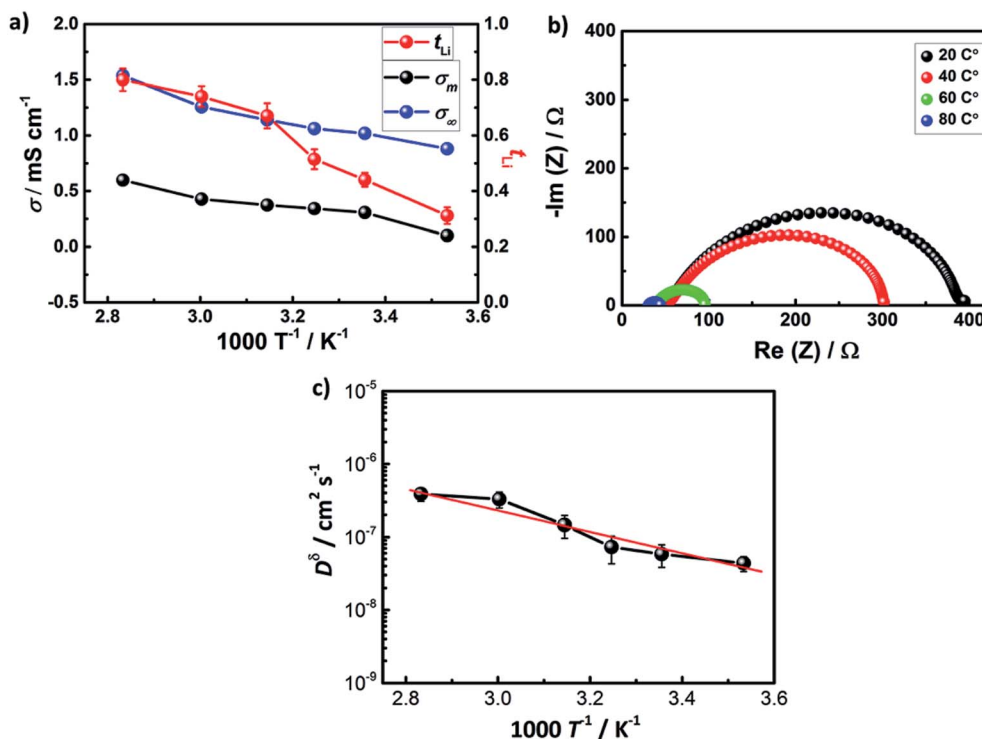
Fig. 3 Temperature-dependent electrochemical properties of AAO: (1 M LiTf/triglyme) electrolyte in an anion blocking Li|electrolyte|Li cell: (a) ionic conductivity (black) and lithium transference number measured by galvanostatic polarization (red). For comparison purposes, ionic conductivity of pure LiTf/triglyme is also shown (blue). The error bars for conductivity measurements correspond to the data point sizes, (b) solid electrolyte interphase (SEI) resistance decrease at elevated temperatures, (c) changes of the lithium salt diffusion coefficient determined at long galvanostatic polarization times. Red line represents a linear fit of the experimental data.

This journal is © The Royal Society of Chemistry 2019

J. Mater. Chem. A, 2019, 7, 13331–13338 | 13333

3. Results and discussion

In the present study, AAO membranes with high pore density, controlled pore size, shape and orientation as illustrated in the SEM image in Fig. 1a, have been employed as the solid part of the liquid–solid electrolyte. The pores of the AAO membrane have conical frustum form with an average upper base radius of 20 nm and a 200 nm lower base radius, Fig. 1a, left. Using the given geometry and the approximate number of pores observed in the SEM micrographs, a surface area value of $A_{calc} = 35$ m^2 g^{-1} can be estimated (available in the ESI†). Additionally, the Brunauer–Emmet–Teller (BET) surface area is measured to be of a similar order of magnitude, $S_{BET} = 24$ m^2 g^{-1}. X-ray diffraction patterns of the AAO membrane asserts the amorphous nature of the Al$_2$O$_3$ material, Fig. 1b.

In ^{1}H magic-angle spinning nuclear magnetic resonance (MAS-NMR) spectra of the crushed AAO samples, a broad chemical shift is observed around 5 ppm, Fig. 1c. This shift can be fitted by three Gaussian components corresponding to the protons in physically adsorbed water ($\delta = 5.9$ ppm, green dotted line) and to the –OH groups bound to aluminum ($\delta = 3.5$ ppm and $\delta = 1.3$ ppm, purple and blue dotted line), giving a total number of 2.4×10^{20} –OH per g^{-1}. The total density of the –OH groups is calculated to be 6 nm^{-2}, taking into account the total number of –OH groups from ^{1}H MAS-NMR and the calculated surface area, A_{calc}. The predominant adsorption of Tf$^-$ anion on the AAO surface in contact with 1 M LiTf/triglyme is expected to lead to an interfacial (or "soggy sand") effect.[33] Indeed, the effective surface zeta potential (ζ_{eff}) of crushed 1 vol% AAO particles dispersed in 1 M LiTf/triglyme electrolyte is negative, $\zeta_{eff} = -28$ mV ($\zeta_{eff} = -6$ mV in 0.2 LiTf/triglyme). However, when the activity of the –OH groups (surface deprotonation) of crushed AAO membranes was probed by potentiometric titrations, values of IEC = 7.2×10^{-2} mmol g^{-1} are measured, an order of magnitude lower than what has been observed for porous SiO$_2$ particles in a similar solvent.[38] With this in mind, the interfacial effect in AAO: glyme electrolytes is expected to be milder than in the SiO$_2$: glyme-based lithium electrolytes. The AAO: (1 M LiTf/triglyme) electrolyte appears transparent (Fig. S1†) despite its relatively high volume fraction of Al$_2$O$_3$ solid, $\varphi = 0.24$, and has thermal properties which are comparable to the pure 1 M LiTf/triglyme.

The lithium transference number of AAO: (LiTf/triglyme) was measured using the galvanostatic polarization method as reported previously.[34] In such a measurement, the salt concentration gradient establishes eventually upon applying constant current and at the steady state, the voltage response results solely from the cation (lithium) transport. The contributions of other resistances to the overall voltage increase, such as the resistances of the passivation layers (solid electrolyte interphase, SEI) formed on the lithium electrodes, should also be considered. The lithium transference number can subsequently be calculated from:

$$t_{Li} = \frac{IR_{tot,0} - IR_{SEI,0}}{U_\infty - IR_{SEI,\infty}}, \tag{1}$$

where I is the constant current applied, $R_{tot,0}$ is the total cell resistance before the galvanostatic polarization, U_∞ is the steady state voltage and $R_{SEI,0}$, $R_{SEI,\infty}$ are the SEI resistances before and after the polarization, respectively. As seen in the Fig. 2a, galvanostatic polarization of AAO: (1 M LiTf/triglyme) electrolyte is a fast process, reaching the steady state after just 200 s, a consequence of the comparatively thin electrolyte. As predicted from the AAO morphology, surface area and the quantity of active –OH groups, lithium transference number calculated using eqn (1) results in $t_{Li} = 0.48$, considerably higher value than the transference number of the pure liquid electrolyte, $t_{Li} = 0.15$, at same salt concentration (Fig. S4†).

The semicircle observed in Fig. 2b corresponds to the SEI formed on the lithium metal surface in contact with the liquid part of the electrolyte. Such SEI appears to be stable during the polarization process with approximate thickness around 10 nm, when calculated for the approximate dielectric constant $\varepsilon \approx 10$ (calculation available in ESI†). Thus, even though the t_{Li} values reported are of the same order as previously seen for liquid lithium electrolytes, the composite appears more promising due to its stability vs. lithium. Furthermore, the $U(t)$ curve exhibits a clear exponential behavior for longer times, enabling us to determine the LiTf salt diffusion coefficient from

$$D^\delta = \frac{l^2}{\tau^\delta \pi^2}, \tag{2}$$

l being the electrolyte thickness (here corresponding to the thickness of AAO), and τ^δ being the time constant of the stoichiometry polarization. The time constant is determined from a linear fit of the $\ln|U - U_\infty|$ vs. t dependence, as seen in Fig. 2c. The corresponding $D^\delta = 4 \times 10^{-8}$ cm^2 s^{-1} is consistent with the values reported previously in a composite mesoporous SiO$_2$: (1 M LiTf/diglyme) liquid/solid electrolyte.[34] The polarization experiments are reproducible, giving analogous values for lithium transference number, room temperature ionic conductivity and salt diffusion coefficient (ESI†). Additionally, an enhancement of t_{Li} from the very low values of 0.006 to 0.03 has been observed in the AAO: 1-methyl-1-propylpiperidinium bis(trifluoromethylsulfonyl)imide ionic liquid containing 0.2 M LiTf (Fig. S6†). Although the improvement of t_{Li} in the solid–liquid composite electrolytes in the current case is still lower than observed in the mesoporous SiO$_2$: (1 M LiTf/diglyme) due to the lower surface area and lower IEC of AAO, the reproducibility of pore structure provide means to systematically investigate the influence of other parameters on the lithium transference number and ionic conductivity, including concentration and temperature.

Fig. 3a shows ionic conductivity and lithium transference number in AAO: (1 M LiTf/triglyme) electrolyte in the temperature range from 10 to 80 °C, where the conductivity of the composite liquid/solid electrolyte improves from 1.8 to 2.6 mS cm^{-1}. The ratio of the ionic conductivity of the liquid/solid composite and the bulk liquid electrolyte stays constant in the entire temperature range ($\sigma_m/\sigma_\infty \approx 0.5$), indicating similar conduction mechanisms and partial blocking of some pathways in the liquid/solid composite electrolyte. Indeed, it is even visible from the SEM that not all of the pores in AAO are continuous and interconnected. A more drastic effect has been observed for the lithium transference number of the liquid/

13334 | J. Mater. Chem. A, 2019, 7, 13331–13338

This journal is © The Royal Society of Chemistry 2019

solid composite, leading to the highest value of $t_{Li} = 0.80$ at 80 °C. This can be explained either by activation of additional surface –OH groups of AAO and/or through changes in the molecular speciation in the liquid electrolyte upon heating, investigated using temperature controlled IR spectroscopy (Fig. S2†). Indeed, temperature increase enhances the ion-pair association to ion pairs and dimers in 1 M LiTf/triglyme (similarly as in LiTf/diglyme[38,39]). The strong solvation of free ions (about 3 glyme molecules) causes endothermic association reaction and entropy gain through association. The result is a stronger interfacial effect and high t_{Li} in AAO: (1 M LiTf/triglyme). At higher temperatures, the increase in ionic conductivity accompanied with the depression in concentration of free ions implies a total mobility increase about 4 times. This is in line with the observed viscosity increase in liquid 1 M LiTf/triglyme (Fig. S3†).

With increasing temperature, a substantial depletion of the resistance of the SEI layer, R_{SEI}, is observed, Fig. 3b, suggesting its chemical composition or morphological changes. This specific point will be discussed in the subsequent work. Following the mobility trend, salt diffusion coefficient, D^{δ}, increases an order of magnitude in the chosen temperature range (Fig. 3c).

Fig. 4a shows the effect of salt concentration on room temperature ionic conductivity and lithium transference number in AAO: LiTf/triglyme. A sharp rise (about 2 orders of magnitude) in the ionic conductivity of liquid/solid composite electrolyte upon increasing concentration from 0.02 M to 0.4 M is observed, followed by a plateau and a drop at high salt concentrations.

To discuss the interfacial effect in the present system, two extreme cases of strong and weak anion adsorption can be considered. In the case of weak anion adsorption, space charge effects are negligible and – if all pathways percolating – the conductivity of the composite is simply given by

$$\sigma_m = (1 - \varphi)\sigma_{\infty}, \qquad (3)$$

where σ_{∞} is the bulk liquid conductivity. The slope of the concentration dependent conductivity and the lithium transference number remains identical to the liquid system. For AAO: LiTf/triglyme, a conductivity of 76% of the bulk liquid is expected (24% depression of the bulk).

In the case of strong anion adsorption on AAO, for sufficiently high surface area, we can assume that all the anions are adsorbed, including the ones in the ion pairs. The cations are then all in the space charge zones. As we can neglect bulk contribution, the conductivity of the composite can be written as

$$\sigma_m = (1 - \varphi)c_{salt}u_+, \qquad (4)$$

where u_+ is the mobility of lithium ions in the pure liquid electrolyte. Here we assume that the mobility of free lithium
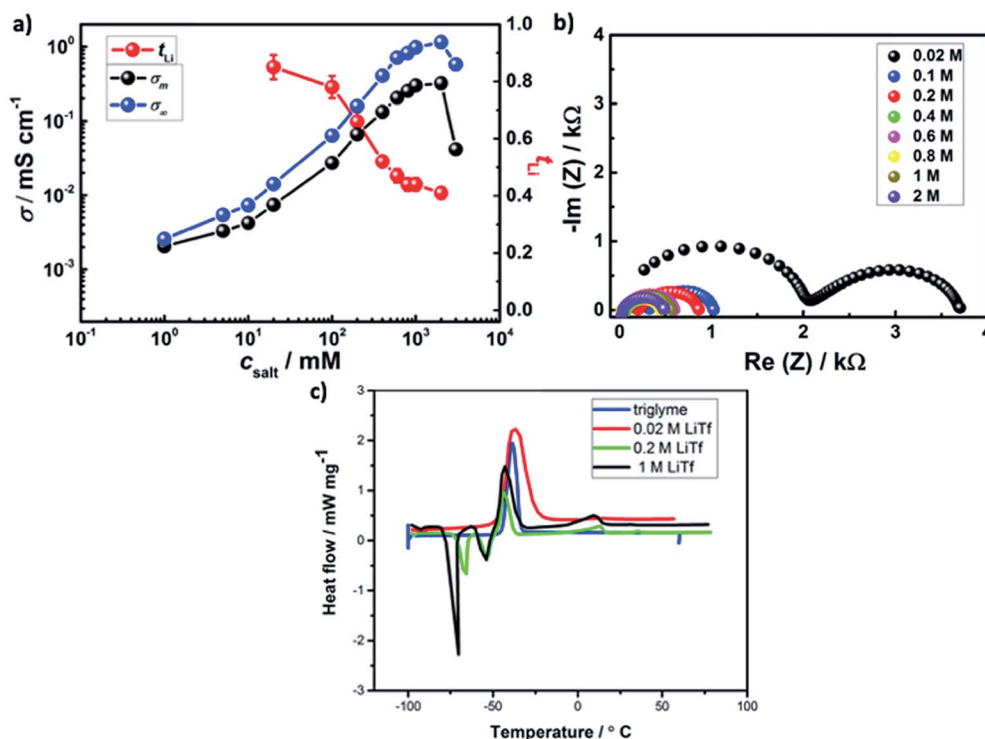

Fig. 4 Lithium salt concentration variation in AAO: (LiTf/triglyme) electrolyte influence on: (a) ionic conductivity (black) and lithium transference number (red) measured by galvanostatic polarization. For comparison purposes, ionic conductivity of pure LiTf/triglyme is also shown (blue). When not marked, the error bars correspond to the size of data points, (b) solid electrolyte interphase resistance. In the case of diluted electrolyte (0.02 M), the high frequency semicircle corresponds to the bulk electrolyte resistance. (c) Thermal properties as measured by differential scanning calorimetry.

ions in the space charge zone (double layer) is equal to the mobility of free lithium in the bulk liquid electrolyte. On the other hand, the conductivity of the bulk liquid can be written as

$$\sigma_\infty = c_+(u_+ + u_-) \quad (5)$$

The values of c_+ can be taken from the previous measurements of the triflate stretching band by infrared spectroscopy, while the mobilities can be taken from the deconvoluted contributions of specific ions to the overall conductivity (σ_+, σ_-) leading to values of $\sigma_m/\sigma_\infty \approx 0.15$ at 1 M LiTf and $\sigma_m/\sigma_\infty \approx 0.5$ at 0.2 M LiTf.[38] In the case of strong adsorption, transference number of 1 is expected.

As the conductivity and lithium transference number are in between the cases of weak and strong adsorption, medium level of adsorption appears to be relevant. A more precise approach would require more information than available. The ratio of the ionic conductivity of the bulk and the ionic conductivity of the liquid/solid composite varies from of $\sigma_m/\sigma_\infty = 0.8$ for 0.02 M LiTf to $\sigma_m/\sigma_\infty = 0.3$ at 1 M LiTf, suggesting stronger adsorption at low c_{salt} and milder adsorption at high c_{salt}. Following the weakening of the adsorption trend, the lithium transference number significantly decreases upon salt addition from $t_{Li} = 0.85$ at 0.02 M to $t_{Li} = 0.52$ at 0.4 M, and the trend continues with somewhat lower rate at higher salt concentrations.

At lower salt concentrations, an additional semicircle corresponding to the electrolyte bulk appears (Fig. 4b). On the other hand, the SEI thickness rises to $d \approx 40$ nm. Interestingly, the DSC spectra of AAO: 0.02 M LiTf/triglyme is drastically different to other liquid–solid electrolytes with salt concentration between 0.2–1 M (Fig. 4c) and is almost identical to the DSC of pure triglyme.

To further investigate the cyclability of this class of electrolytes in the symmetric lithium cells, a cyclic lithium plating–stripping procedure consisting of one hour cell charging followed by one hour discharging was employed. Fig. 5 illustrates the time-dependent voltage profile under constant current density of 0.3 mA cm^{-2} for a Whatman glass fiber separator infiltrated with 1 M LiTf/triglyme, and AAO: 0.02 M LiTf/triglyme electrolyte, respectively. The voltage response of a Whatman glass fiber separator infiltrated with 1 M LiTf/triglyme increases linearly in time to values as high as 0.5 V after 300 hours. In contrast, the AAO: 1 M LiTf/triglyme shows no gradual voltage increase, and voltage stabilizes with time achieving values of 0.1 V at the end of the stripping–platting procedure (see inset). However, sudden and momentary instabilities can be observed in the case of AAO: 1 M LiTf/triglyme. This may be consequence of the blocking of some pores and appearance of local short circuits due to the electrolyte and/or salt decomposition.[40] Such behavior has been observed for both liquid electrolytes infiltrated in separator as well as in solid electrolytes with highly stable SEIs and does not interfere with long-term electrolyte performance.[41] The cell failure in the AAO:
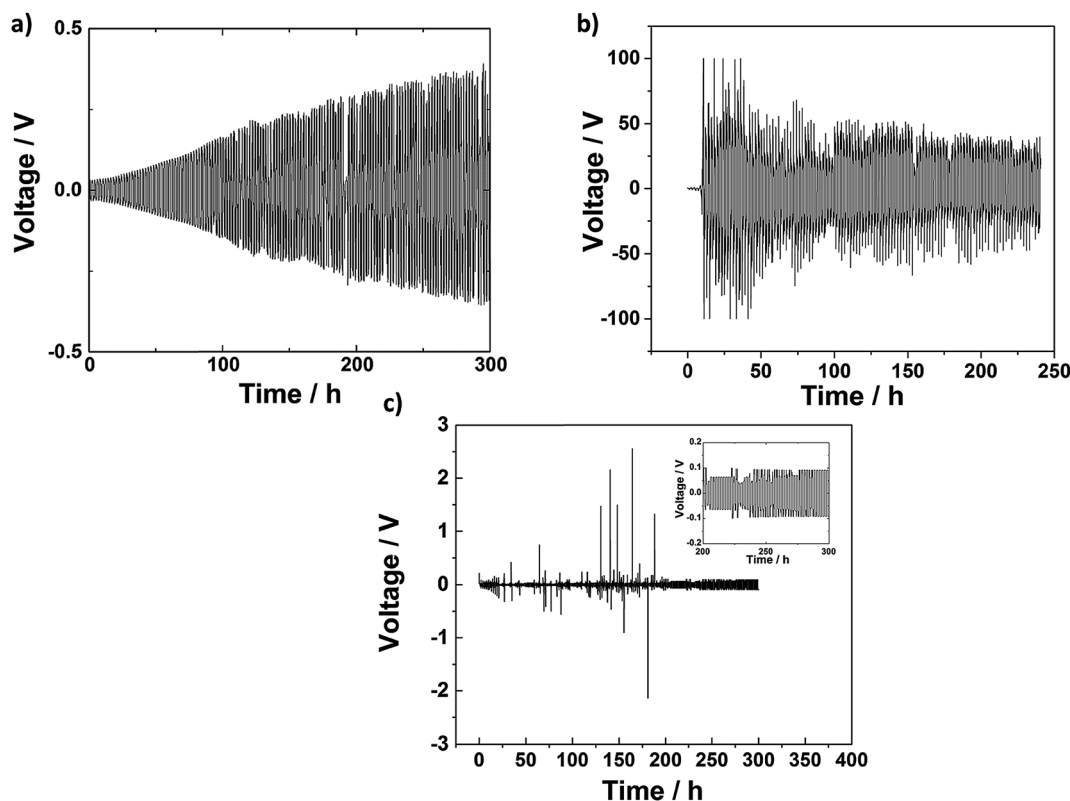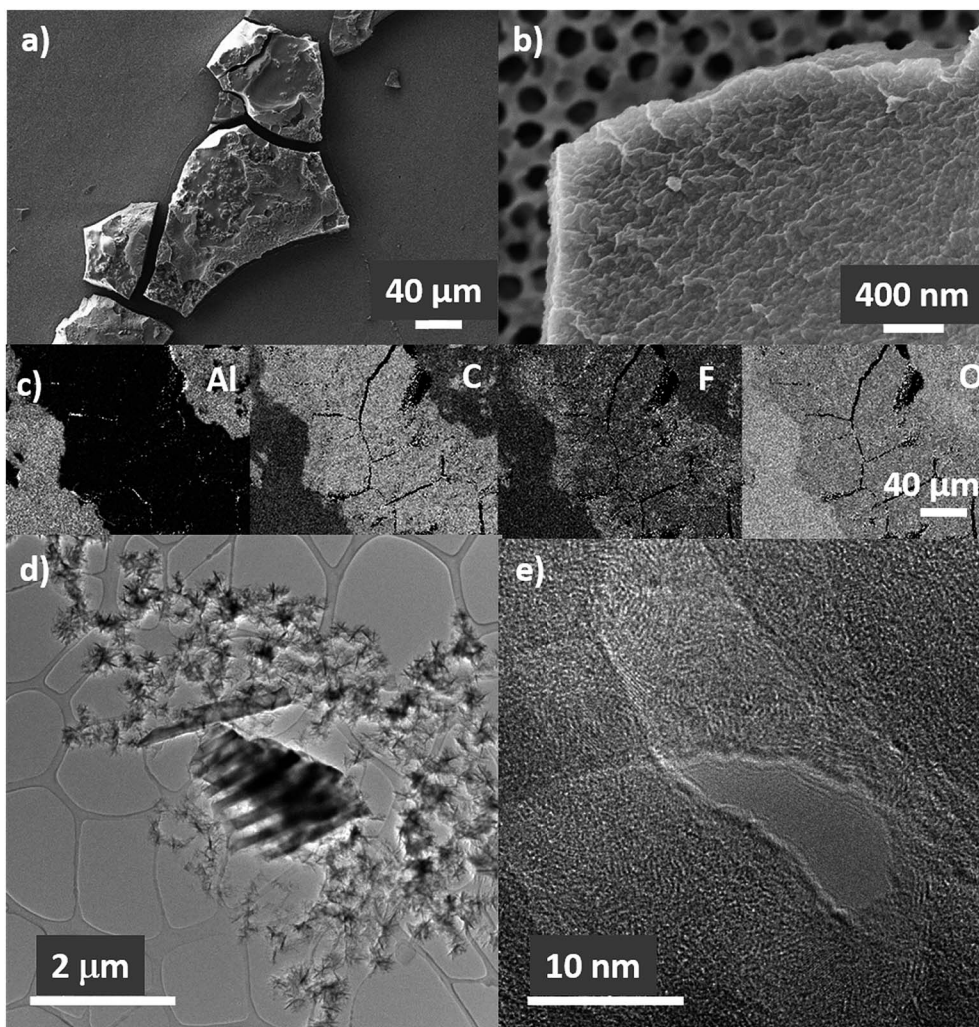

Fig. 5 Voltage–time profiles during electrochemical stripping–platting experiments at 0.3 mA cm^{-2} current density in a symmetrical Li|electrolyte|Li cell with different electrolytes: (a) 1 M LiTf/triglyme infiltrated into a Whatman glass fiber separator, (b) AAO: (0.02 M LiTf/triglyme) (c) AAO: (1 M LiTf/triglyme). The inset shows stable behavior at long stripping–platting times.

13336 | *J. Mater. Chem. A*, 2019, **7**, 13331–13338

This journal is © The Royal Society of Chemistry 2019

Fig. 6 Micrographs of the lithium deposit formed during the stripping–platting experiment in Li|AAO: (1 M LiTf/triglyme)|Li cell experiments at 0.3 mA cm^{-2} current density: (a and b) scanning electron micrographs of the lithium deposit on the surface of porous AAO (c) corresponding energy-dispersive X-ray spectroscopy (EDS) elemental mapping images. The element under study corresponds to the lighter part of the EDS recorded, (d and e) transmission electron micrographs of the lithium deposit. Clear lattice fringes at higher magnification confirm the crystallinity of the material.

1 M LiTf/triglyme electrolyte seems to occur later than its AAO-free counterpart, suggesting that liquid–solid are able to partially hinder dendrite formation and substantially enhance the lifetime of the cell. On the other hand, one might expect that the AAO: 0.02 M LiTf/triglyme would show the best stripping/plating behavior since there the lithium transference number is the highest. This has however not been experimentally confirmed and is most probably the consequence of unstable SEI in the electrolytes with low salt concentration, inducing dendrite formation.[42]

Growth of lithium deposits in the form of mossy lithium can be observed by *ex situ* SEM after disassembling Li|AAO: (1 M LiTf/triglyme)|Li cell both on the surface of lithium and on the AAO (Fig. 6a–c). The deposits are large particles (*ca.* 100 μm long), covered by a thin SEI layer. This is confirmed by energy-dispersive X-ray spectroscopy (EDS) elemental mapping images (Fig. 6c) showing that C, F, and O elements are evenly distributed on the particle surface. The structure of the deposit appears to be crystalline (Fig. 6d and e), with clear lattice fringes visible in high resolution TEM. However, the amount of the crystalline phase is not large enough to be detected by the XRD measurements. Such deposits might lead to cell short circuit if they penetrate the full length of AAO.

4.   Conclusions

In this study, we report on LiTf/triglyme infiltrated in porous AAO as a possible electrolyte for lithium metal batteries. The beneficial adsorption of the anion on the surface of AAO leads to the increase of lithium transference number, t_{Li}. The interfacial effect on the surface is higher at lower salt concentration and elevated temperature, with t_{Li} reaching values of 80% at 80 °C in 1 M LiTf/triglyme, and 85% at room temperature in 0.02 M LiTf/triglyme. Interestingly, glyme-based AAO electrolyte seems to

combine high lithium transference numbers with good stability with lithium electrodes.

Glyme-based liquid–solid electrolytes proved to be more successful in stopping dendrite growth compared to their liquid counterparts infiltrated in glass fiber separators. However, at long stripping/plating times, mossy crystalline lithium deposits covered by an SEI can still be observed.

Conflicts of interest

There are no conflicts to declare.

Acknowledgements

References

1 J.-M. Tarascon and M. Armand, *Nature*, 2001, **414**, 359–367.

2 W. Xu, J. Wang, F. Ding, X. Chen, E. Nasybulin, Y. Zhang and J.-G. Zhang, *Energy Environ. Sci.*, 2014, 7(2), 513–537.

3 K. Zhang, G.-H. Lee, M. Park, W. Li and Y.-M. Kang, *Adv. Energy Mater.*, 2016, 6(20), 1600811.

4 M. Tikekar, S. Choudhury, Z. Tu and L. Archer, *Nat. Energy*, 2016, **1**, 16114.

5 D. Lin, Y. Lui and Y. Cui, *Nat. Nanotechnol.*, 2017, **12**, 194–206.

6 H. Kim, G. Jeong, Y.-U. Kim, J.-H. Kim, C.-M. Park and H.-J. Sohn, *Chem. Soc. Rev.*, 2013, **42**, 9011–9034.

7 X.-B. Cheng, J.-Q. Huang and Q. Zhang, *J. Electrochem. Soc.*, 2018, **165**, A6058–A6072.

8 R. Bhattacharyya, B. Key, H. Chen, A. S. Best, A. F. Hollenkamp and C. P. Grey, *Nat. Mater.*, 2010, **9**, 504.

9 J. Wandt, C. Marino, H. A. Gasteiger, P. Jakes, R.-A. Eichel and J. Granwehr, *Energy Environ. Sci.*, 2015, **8**, 1358.

10 M. Wu, Z. Wen, Y. Liu, X. Wang and L. Huang, *J. Power Sources*, 2011, **196**(11), 8091–8097.

11 G. Zheng, S. W. Lee, Z. Liang, H.-W. Lee, K. Yan, H. Yao, H. Wang, W. Li, S. Chu and Y. Cui, *Nat. Nanotechnol.*, 2014, **9**, 618–623.

12 N.-W. Li, Y.-X. Yin, C.-P. Yang and Y.-G. Guo, *Adv. Mater.*, 2016, **28**, 1853–1858.

13 A. Kozen, C.-F. Lin, O. Zhao, S. B. Lee, G. Rubloff and M. Noked, *Chem. Mater.*, 2017, **29**, 6298.

14 G. Wan, F. Guo, H. Li, Y. Cao, X. Ai, J. Qian, Y. Li and H. Yang, *ACS Appl. Mater. Interfaces*, 2018, **10**(1), 593–601.

15 C.-P. Yang, Y.-X. Yin, S.-F. Zhang, N.-W. Li and Y.-G. Guo, *Nat. Commun.*, 2015, 8058.

16 Q. Yun, Y.-B. He, W. Lv, Y. Zhao, B. Li, F. Kang and Q.-H. Yang, *Adv. Mater.*, 2016, **28**(32), 6932–6939.

17 L.-L. Lu, J. Ge, J.-N. Yang, S.-M. Cheng, H.-B. Yao, F. Zhou and S.-H. Yu, *Nano Lett.*, 2016, **16**(7), 4431–4437.

18 C. Monroe and J. Newman, *J. Electrochem. Soc.*, 2005, **152**, A396–A404.

19 R. Khurana, J. Schaefer, L. Archer and G. Coates, *J. Am. Chem. Soc.*, 2014, **136**(20), 7395–7432.

20 S.-O. Tung, S. Ho, M. Yang, R. Zhang and N. Kotov, *Nat. Commun.*, 2015, **6**, 6152.

21 C. Xu, Z. Ahmad, A. Aryanafar, V. Viswanathan and J. Greer, *Proc. Natl. Acad. Sci. U. S. A.*, 2017, **114**(1), 57–61.

22 L. Gireaud, S. Grugeon, S. Laruelle, B. Yrieix and J.-M. Tarascon, *Electrochem. Commun.*, 2006, **8**(10), 1639–1649.

23 S.-K. Jeong, H.-Y. Seo, D.-H. Kim, H.-K. Han, J.-G. Kim, Y. Lee, Y. Iriyama, T. Abe and Z. Ogumi, *Electrochem. Commun.*, 2008, **10**(4), 635–638.

24 J. Stark, Y. Ding and P. Kohl, *J. Electrochem. Soc.*, 2011, **158**(10), A1100–A1105.

25 G. Lane, A. Best, D. MacFarlane, M. Forsyth and A. Hollenkamp, *Electrochim. Acta*, 2010, **55**(6), 2210–2215.

26 L. Suo, Y.-S. Hu, H. Li, M. Armand and L. Chen, *Nat. Commun.*, 2013, **4**, 1481.

27 R. Bouchet, S. Maria, R. Meziane, A. Aboulaich, L. Lienafa, J.-P. Bonnet, T. Phan, D. Bertin, D. Gigmes, D. Devaux, R. Denoyel and M. Armand, *Nat. Mater.*, 2013, **12**, 452–457.

28 Y. Lu, Z. Tu and L. Archer, *Nat. Mater.*, 2014, **13**, 961–969.

29 Z. Tu, M. Zachman, S. Choudhury, S. Wei, L. Ma, Y. Yuang, L. Kourkoutis and L. Archer, *Adv. Energy Mater.*, 2017, 7(8), 1602367.

30 J.-K. Kim, D. Kim, S. Joo, B. Choi, A. Cha, K. Kim, T.-H. Kwon, S. Kwak, S. Kang and J. Jin, *ACS Nano*, 2017, **11**(6), 6114–6121.

31 J. Jorne, *Nano Lett.*, 2006, **6**(12), 2973–2976.

32 C. Pfaffenhuber, F. Hoffmann, M. Fröba, J. Popovic and J. Maier, *J. Mater. Chem. A*, 2013, **1**, 12560.

33 C. Pfaffenhuber, M. Göbel, J. Popovic and J. Maier, *Phys. Chem. Chem. Phys.*, 2013, **15**(42), 18318.

34 J. Popovic, G. Hasegawa, I. Moudrakovski and J. Maier, *J. Mater. Chem. A*, 2016, **4**, 7135.

35 J.-N. Chazalviel, *Phys. Rev. A: At., Mol., Opt. Phys.*, 1990, **42**, 7355.

36 M. Tikekar, L. Archer and D. Koch, *J. Electrochem. Soc.*, 2014, **161**, A847.

37 H. Wang, M. Matsui, H. Kuwata, H. Sonoki, Y. Matsuada, X. Shang, Y. Takeda, O. Yamamoto and N. Imanishi, *Nat. Commun.*, 2017, **8**, 15106.

38 M. Petrowsky, R. Frech, S. N. Suarez, J. R. P. Jayakody and S. Greenbaum, *J. Phys. Chem. B*, 2006, **110**(46), 230.

39 J. Popovic, C. Pfaffenhuber, J. Melchior and J. Maier, *Electrochem. Commun.*, 2015, **60**, 195.

40 G. Girard, M. Hilder, D. Nucciarone, K. Whitbread, S. Zavorine, M. Moser, M. Forsyth, D. MacFarlane and P. Howlett, *J. Phys. Chem. Lett.*, 2017, **121**, 21087.

41 Q. Pang, X. Liang, A. Shyamsunder and L. Nazar, *Joule*, 2017, **1**(4), 871.

42 M. Nojabaee, K. Müller, B. Fenk, U. Starke, J. Popovic and J. Maier, in preparation.

13338 | *J. Mater. Chem. A*, 2019, **7**, 13331–13338

This journal is © The Royal Society of Chemistry 2019